Wideband Characterization of a Typical Bonding Wire for Microwave and Millimeter-wave Integrated Circuits

Hai-Young Lee, *Member, IEEE*

Abstract—**A typical grounded bonding wire with a minimum total length of 480 μm for MMIC's and OEIC's is characterized using the Method of Moments with the incorporation of the ohmic loss as well as the radiation loss over a wide range of frequencies. The distributed ohmic resistance is calculated by an application of the Phenomenological Loss Equivalence Method. The simulated results show the wire resistance and the inductance are greatly increasing to frequencies above 30 GHz due to the high radiation effect enhanced by the slow-wave effect of the ohmic loss. The bonding wire is highly inductive in most of the frequency range and the maximum quality factor is mostly limited by the ohmic resistance. The results also show the simple static modeling of computer-aided design software that considers only the free-space wire inductance and the skin-effect resistance, overestimates the wire inductance at low frequencies, and is inappropriate at high frequencies due to the high radiation effect. This approach can be applied to many arbitrarily shaped interconnection wires for wideband design and characterization of high-frequency integrated circuits.**

I. Introduction

WIRE bonding has been widely used in fabrication and characterization of monolithic and hybrid integrated circuits for microwave/millimeter-wave and optoelectronics. Recent advances in integration technology and performance of integrated circuits have achieved increased speed and bandwidth, greater integration density, and multi-chip interconnections of integrated devices [1]–[3]. However, in order to keep and externally realize the high performance, internal effects of parasitics and packages—increasingly critical in the high frequency circuits—should be taken into account extensively [4].

The wire bonding effect, one of the dominant parasitic effects under high-frequency circumstances, must be taken into account from the beginning of the circuit design while wire bonding is in general the last one in the device fabrication procedures [5]. Furthermore, recent technologies of computer-aided design (CAD) and characterization of the high-frequency devices and circuits have a tendency to rely on real measurements using advanced network analyzers and improved calibration methods that mostly require wire bonds and their accurate characterization for launching and probing [6]. However, real measurements of the bonding wire characteristics for accurately de-embedding the device characteristics are difficult in most circumstances involving tiny geometries and their corresponding crosstalk problems.

Wideband characterization of the bonding wire has not been extensively treated and in open literature, except for the simple modeling of skin-effect resistance and the static description of free-space wire inductance [7]. A static conformal mapping approach has been introduced for an infinitely-long wire located above a grounded substrate in which the effective dielectric constant and the characteristic impedance are calculated with no ohmic and radiation losses incorporated [8], [9].

In this paper, the Method of Moments (MoM) is applied to a typical bonding wire geometry of a minimum 480 μm total length with the incorporation of the wideband ohmic resistance and internal inductance using the Phenomenological Loss Equivalence Method (PEM) [10]. High radiation resistance and increasing inductance enhanced by the slow-effect of the ohmic loss have been observed above 30 GHz. The simulated results show computer-aided design software, which considers only the free-space static wire inductance and the skin-effect resistance, overestimates the wire inductance at low frequencies and is inappropriate at high frequencies due to the high radiation effect. The high radiation critical for designing and packaging high-frequency integrated circuits can be minimized mainly by reducing the bonding wire height from the bonding pad. The bonding wire is highly inductive in most of the frequency range (DC to 100 GHz) while the maximum quality factor is limited by the ohmic loss. This wideband characterization of the typical grounded bonding wire is expected to be helpful for accurate design and characterization of high frequency MMIC's and OEIC's. Finally, this approach, including both wideband ohmic and radiation losses, can be widely applied to wideband characterization of many arbitrarily shaped interconnection wires for high-frequency integrated circuits.

II. Description and Modeling of a Typical Grounded Bonding Wire

Ball-bonding is considered for its popularity and reliability. Wedge-bonding, however, is relatively less popular and reliable since substrate heating and high bonding pressure can result in device degradations as well as damage incidental to the bonding pad in some circumstances [11]. On the other

Manuscript received April 14, 1993; revised February 22, 1994. This work was supported by NON-DIRECTED RESEARCH FUND, the Korea Research Foundation, 1993, and the University Research Fund, Ajou University, 1992.

H.-Y. Lee is with the Department of Electronics Engineering, Ajou University, Suwon 441-749, Korea.

IEEE Log Number 9406821.

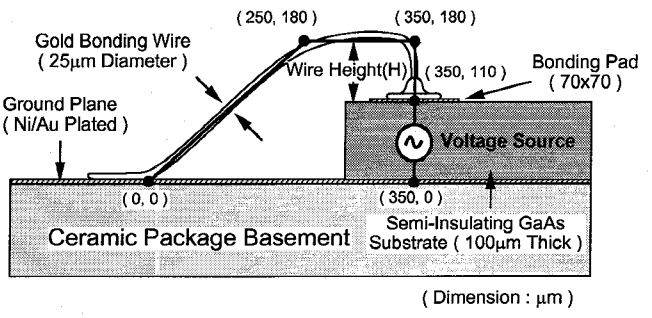

Fig. 1. Typical geometry of a grounded ball-bonding wire on a 100-μm GaAs substrate with a minimum 480 μm total length statistically obtained by bonding experiments.

hand, wedge-bonding has an advantage of less wire inductance because of the shorter wire length.

The typical shape of a grounded bonding wire shown in Fig. 1 has been statistically obtained from real wire bonding experiments of a 25-μm-diameter gold wire under a ball-bonding machine with a 38-μm hole-diameter capillary. A minimum total length of the bonding wire (480 μm) has been obtained from an optimum setting of the bonding machine. Total height of the bonding step is about 110 μm for the 100-μm GaAs substrate thickness and the 10-μm die-attachment thickness, which are typical of monolithic integrated circuits based on a GaAs substrate [12]. The bonding wire crest is at a height of 70 μm from the bonding pad.

A. Ohmic Resistance Modeling by the PEM

The distributed ohmic resistance and internal inductance have been calculated in a wide range of field penetration using the Phenomenological Loss Equivalence Method, which has been applied for a microstrip line using a normal conductor or a superconductor [10] and experimentally confirmed for coplanar and coplanar slow-wave structures [13]. The PEM is originally based on inherent field penetration properties of a planar quasi-TEM line in which surface current distribution on the entire conductor circumference is almost constant for any field penetration and the fields always penetrate in the normal direction of the conducting surface. Since the surface current density of the round bonding wire is uniform along the thin wire circumference at any field penetration as well, cross-sectional distribution of the longitudinal current penetrated inside the bonding wire can be approximately modeled by the PEM based on the same field penetration properties. Transverse resonance effect of the penetrated fields in thin planar quasi-TEM lines [14] is not significant in this circular bonding wire and hence is expected in this PEM calculation to lower the estimation of the round wire resistance around the transverse resonant frequency of the bonding wire.

Using the inherent field penetration properties of a quasi-TEM line, the PEM can approximately model an infinite bonding wire in free-space by the equivalent single strip in terms of the equivalent ohmic loss. The equivalent strip width for a bonding wire with a radius a in free-space

$$W_e = 1/G = 2\pi a \tag{1}$$

is obtained from the defined geometric factor (G) by equating the skin-effect resistance to that of the original line at very shallow penetration. The thickness of the equivalent strip

$$t_e = AG \tag{2}$$

is calculated from the same ohmic resistance at complete penetration, where A is the effective cross-section area at complete penetration (i.e., $A = \pi a^2$ for the infinite bonding wire in free-space). Then, the distributed internal impedance of the equivalent strip (Z_i) can be simply calculated by

$$Z_i = R_i + j\omega L_i = Z_s G \coth(\sigma Z_s A G) \tag{3}$$

where Z_s and σ are the surface impedance and the conductivity of the same conducting material. The calculated internal impedance (Z_i) is incorporated in the linearized-wire modeling of the MoM by appropriately distributing the internal impedance on pulse segments of the bonding wire using the lumped impedance loading method [15].

B. MoM Formulation Using a Linearized-Wire Model

The impedance analysis of the bonding wire is formulated using the well-known Galerkin's method [15] with pulse basis and pulse testing functions. The bonding wire is described by a linearized-wire model with three linear wires of total 12 pulse segments as shown in Fig. 1. This wire segmentation, corresponding to the minimum 72 pulses per wavelength in the whole frequency range considered, is adequate to the impedance modeling with negligible segmentation errors in the MoM calculation. The dielectric effect of the semi-insulating GaAs substrate and the bonding pad capacitance have been neglected for the simplification of the MoM formulation. A difficulty in including the dielectric effect into the MoM formulation comes from the unknown Green's function for the inhomogeneous geometry. Since the substrate modes can be generated above few hundred GHz and the magnetic field dominates over the electric field for the very low impedance wire, the dielectric effect is expected to be small for the impedance calculation in the frequency range considered.

Since the radius of the bonding wire (12.5 μm) is very small compared to the wire length and the wavelength in the whole frequency range, we can assume the axial current ($I(s)\hat{s}$)) is only directed along the wire axis($\hat{s}$). Using the Lorentz gauge condition, the electric field ($\vec{E}_s$) scattered by the unknown current can be expressed by the vector potential ($\vec{A}$) and the scalar potential (Φ) in terms of the free-space Green's function as follows, where the charge distribution ($q(s)$) is related to the current distribution ($I(s)$) by the continuity equation.

$$\vec{E}_s = -j\omega\mu\vec{A} - \nabla\Phi \tag{4}$$

$$\vec{A} = \frac{1}{4\pi}\int I(s')\hat{s}(s')k(s-s')\,ds' \tag{5}$$

$$\Phi = \frac{1}{4\pi\varepsilon}\int q(s')k(s-s')\,ds' \tag{6}$$

where

$$q(s) = \frac{1}{-j\omega}\frac{dI}{ds}$$

$$k(s-s') = \frac{1}{2\pi}\int_{-\pi}^{\pi}\frac{e^{-jkr}}{r}\,d\phi$$

$$r = \left((s-s')^2 + 4a^2\sin^2\frac{\phi}{2}\right)^{(1/2)}$$

In the above equations, s' and s are the source and the field points on the wire axis and the kernel ($k(s-s')$) is represented by the integration of the Green's function on the whole wire circumference. Assuming a perfectly conducting wire, we can impose the zero boundary condition of total tangential electric field on the conductor surface. Hence, the incident field ($\vec{E}_i$) can be represented by the integral equation of

$$-\vec{E}_i\cdot\hat{s} = -j\omega\mu\vec{A}\cdot\hat{s} - \hat{s}\cdot\nabla\Phi = \vec{E}_s\cdot\hat{s}. \tag{7}$$

The integral equation (7) can be discretized into a matrix form by the well-known Galerkin's process using pulse testing and pulse basis functions. The axial line current ($I(s)$) and the linear charge density ($q(s)$) in (5) and (6) are approximated by a series of pulse expansion functions($p_n(s)$) by dividing the bonding wire into N segments of Δs_n length as follow. The charge segmentation is represented by the current pulse ($p_n(s)$) displaced by a half pulse width ($\Delta s_n/2$) in order to incorporate the continuity equation by a difference approximation.

$$I(s) = \sum_1^N I_n p_n(s) \tag{8}$$

$$q(s) = -\frac{1}{j\omega}\sum_1^N\frac{(I_{n+1}-I_n)}{(s_{n+1}-s_n)}$$

$$p_n(s) = \begin{cases}1 & \text{if } s_{n-(1/2)}<s<s_{n+(1/2)}\\ 0 & \text{otherwise}\end{cases}. \tag{9}$$

Now, by assuming slowly-varying electric field and potential distributions over the pulse segments, we enforce the integral equation (7) at a test segment of s_m using the same pulse testing function p_n(s). Then, the resulting integral equation is discretized at each test segment (s_m) by the current expansion coefficients (I_n) as follows.

$$\vec{E}_i(s_m)\cdot\vec{s}_m = j\omega\mu\vec{A}(s_m)\cdot\vec{s}_m + \Phi(s_{m+(1/2)}) - \Phi(s_{m-(1/2)}) \tag{10}$$

where

$$\vec{A}(s_m) = \frac{1}{4\pi}\sum_1^N I_n\hat{s}_n\int_{s_{n-(1/2)}}^{s_{n+(1/2)}}k(s_m-s')\,ds'$$

$$\Phi(s_{m\pm(1/2)}) = -\frac{1}{j4\pi\omega\varepsilon}\sum_1^N\frac{I_{n+1}-I_n}{s_{n+1}-s_n}\cdot\int_{s_{n-(1/2)}}^{s_{n+(1/2)}}k(s_{m\pm(1/2)}-s')\,ds'$$

The discretized integral equation (10) can be rearranged into the following Kirchhoff's network equation of a NxN square matrix form using the defined integrals ($\Psi_{m,p,q}$).

$$[Z][I] = [V] \tag{11}$$

where

$$Z_{mn} = \frac{1}{j4\pi\omega\varepsilon}\left\{\begin{array}{l}\omega^2\varepsilon\mu[\vec{s}_m\cdot\hat{s}_n]\Psi_{m,n-(1/2),n+(1/2)}\\ -\dfrac{1}{(s_{n+1}-s_n)}[\Psi_{m+(1/2),n,n+1}\\ \qquad -\Psi_{m-(1/2),m,n+1}]\\ +\dfrac{1}{(s_n-s_{n-1})}[\Psi_{m+(1/2),n-1,n}\\ \qquad -\Psi_{m+(1/2),n-1,n}]\end{array}\right\}$$

$$\Psi_{m,p,q} \equiv \int_{s_p}^{s_q}k(s_m-s')\,ds'$$

The applied voltage source at a source segment (V_m) is represented using the delta-gap model of a constant incident tangential electric field between the ground plane and the bonding pad with no fringing. The ground plane, assumed to be perfectly conducting, has been replaced by the image wire using the image theory. Therefore, there are $2N$ segments and $2N$ unknowns to be determined, which can be reduced to N unknowns by adding two columns of the $2N \times 2N$ $[Z]$ matrix corresponding the original and the image currents. The wire connection has been performed by overlapping the current pluses at wire junctions based on the Kirchoff's current law [16]. The internal impedance of the lossy bonding wire calculated by the PEM is appropriately discretized and distributed along the pulse segments by adding the lumped impedance to the corresponding diagonal elements of the impedance matrix. The current distribution for an applied source voltage between the bonding pad and the ground plane has been calculated by the Gauss elimination procedure with partial pivoting. The input impedance of the bonding wire is finally calculated by dividing the applied voltage by the input current at the bonding pad.

III. Distributed Internal Impedance of the Bonding Wire

In Fig. 2, the distributed ohmic resistance of a free-space gold bonding wire calculated by the PEM is compared with analytic expressions for the internal impedance of a round wire [17], with experimental results for a copper wire [18] converted for the gold bonding wire by changing the conductivity and the frequency range, and with simple skin-effect resistance of a commercially available CAD software [19]. At high frequencies with shallow penetration above 1 GHz, they are in very good agreement and closely follow the skin-effect resistance of the CAD software. At very low frequencies below 0.1 GHz, the ohmic resistance is saturated to the DC resistance (50 Ohm/m) due to complete field penetration into the bonding wire.

In the mid-frequency range between 0.1 and 1 GHz, the skin depth becomes comparable to the wire radius as well as the equivalent strip thickness in the PEM. Then, the transverse resonance effect of the penetrated field is observed in the equivalent planar strip of the PEM. The resonance effect results in a small discrepancy of the PEM data from the analytic and experimental data in the mid-frequency range, which can be neglected compared to the high wire reactance contribution. The internal inductance of the bonding wire is observed also saturating below 0.5 GHz due to the saturation

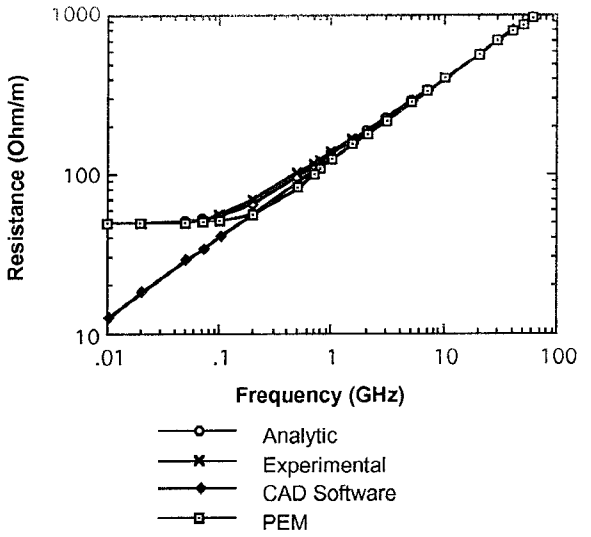

Fig. 2. Distributed ohmic resistances of an infinite gold bonding wire with 25-μm diameter in free-space calculated by analytic expression, experimental results, CAD software, and the PEM.

of the field penetration and being negligibly small compared to the external inductance in the whole frequency range.

IV. Bonding Wire Resistance and Inductance

Total resistance and inductance of the grounded bonding wire shown in Fig. 3 are calculated using the MoM with the incorporation of the ohmic resistance. In Fig. 3(a), the resistances calculated for the cases of lossless and lossy bonding wires have been compared with the skin-effect resistance of the CAD software in which no radiation and field penetration effects are included. It can be observed that the radiation resistance calculated for a lossless bonding wire dominates over the skin-effect resistance above 70 GHz. On the other hand, the pure ohmic resistance, which is almost the same as the skin-effect resistance above 1 GHz, dominates over the radiation resistance at low frequencies.

At high frequencies above 30 GHz, the total resistance of the actual lossy bonding wire is observed to be higher than a simple summation of the ohmic resistance and the radiation resistance that are, respectively, calculated from the distributed ohmic resistance and for a lossless bonding wire. This is due to the slow-wave effect of ohmic loss [20]. The skin-effect loss effectively increases the amplitude and phase variation of the longitudinal current distribution along the actual bonding wire, and hence the consequent radiation becomes higher than that of a lossless bonding wire. The high radiation not only increases the wire impedance, but also enhances the problems of cross-talk and package resonance effects in high-frequency integrated circuits [4].

As shown in Fig. 3(b), the static wire inductance calculated by CAD software is about 15% higher than that of this rigorous calculation at low frequencies. This overestimation comes from the free-space assumption of an infinitely long bonding wire in the CAD software. Therefore, the mutual inductance between the bonding wire and its image contributes about 15% to the total inductance. At high frequencies, the

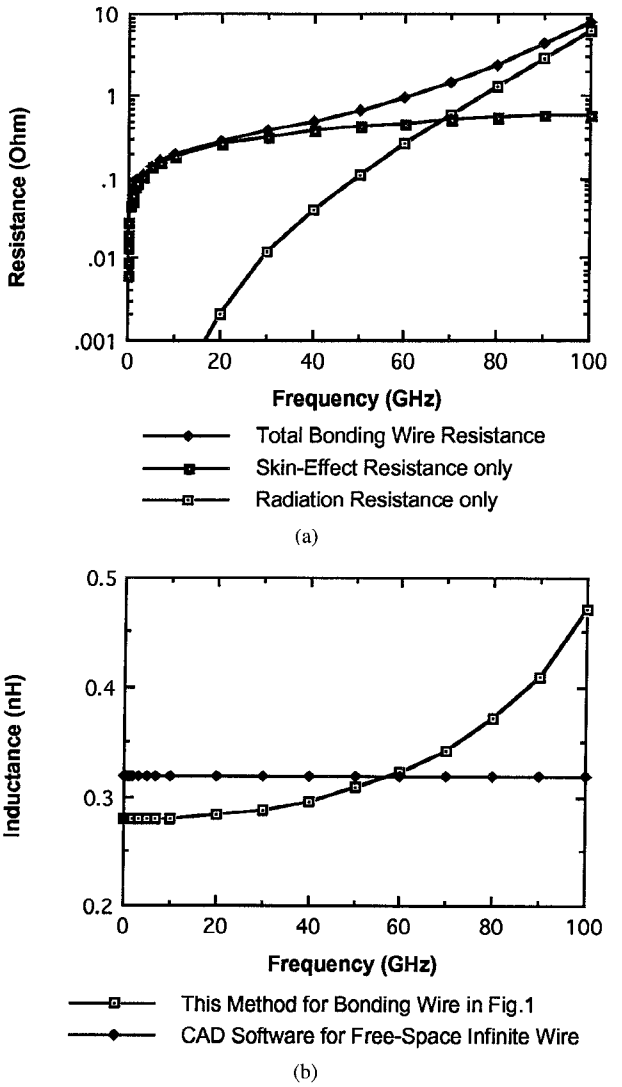

Fig. 3. (a) Radiation, skin-effect, and total resistances and (b) inductances of the grounded bonding wire calculated by the MoM and CAD software.

calculated inductance is rapidly increasing and much higher than the static inductance. The high inductance associated with the radiation effect greatly increases the grounding impedance of the bonding wire and results in a bandwith limitation for high frequency integrated circuits.

In order to see the ohmic loss and radiation loss effects clearly, shown in Fig. 4 are quality factors of lossless and actual lossy bonding wires calculated by the MoM; also shown is that of a free-space bonding wire calculated by CAD software. The quality factor of the actual lossy bonding wire is limited by the ohmic loss at low frequencies and the radiation loss at high frequencies, respectively, and shows the bonding wire highly inductive in most of the frequency range. The maximum quality factor is about 150 at 40 GHz, which is almost the same as that of a 50-Ohm microstrip line [12] and higher than the maximum (50) of integrated inductors [21] on a 100-μm thickness semi-insulating GaAs substrate. Since the ohmic resistance is much higher than the radiation resistance around 40 GHz as shown in Fig. 3(a), the maximum quality factor can be increased mainly by reducing the ohmic resistance using thicker bonding wires and

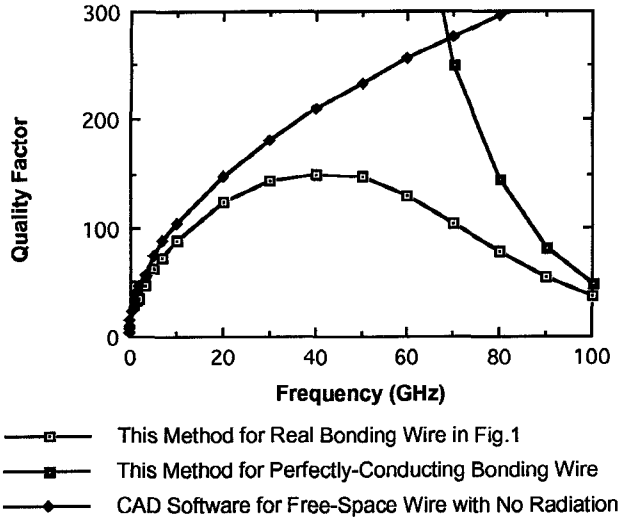

Fig. 4. Quality factors of the lossy and lossless grounded bonding wires (calculated by the MoM) and a free-space infinite bonding wire (calculated by CAD software).

multiple wire bondings. The parallel-LC resonant frequency (97 GHz) between the bonding wire inductance and 0.0058 pF capacitance of a typical 70 μm $\times$ 70-μm bonding pad is far below the self-resonant frequency (147 GHz) of the radiating bonding wire. Therefore, since the parallel resonance greatly increases the grounding impedance around the resonant frequency, the bonding pad area must be minimized to reduce the pad capacitance, and hence increase the resonant frequency, especially for millimeter-wave integrated circuits.

V. Impedance Variation to the Bonding Wire Height

The impedance of a grounded bonding wire is in general dependent on the total length and the shape. At high frequencies, the radiation effect is increasing proportionally to the height of the vertical wire section directly connected to the bonding pad. The other sections are not relatively critical since their current directions are opposite to those of their image sections. Throughout the wire bonding experiments, it was found that the wire height and the substrate thickness are most critical for achieving the minimum total length of the grounded bonding wire as well as bonding repeatability. Therefore, the impedance variation to the bonding wire height are shown in Fig. 5, where the height H from the bonding pad is varied from 70–210 μm and the corresponding total length is also varied from the minimum 480–720 μm. The radiation resistance as well as the inductance are greatly increased for the small variation of the wire height. That is because the self-resonant frequency is inversely proportional to the bonding wire height, and hence the radiation peak at the resonant frequency is moving to lower frequency. Therefore, the bonding wire height should be accurately controlled and minimized in order to reduce the radiation and maintain the bandwidth of high-frequency integrated circuits.

VI. Conclusion

The impedance of a typical grounded bonding wire for MMIC's and OEIC's has been characterized in a wide range

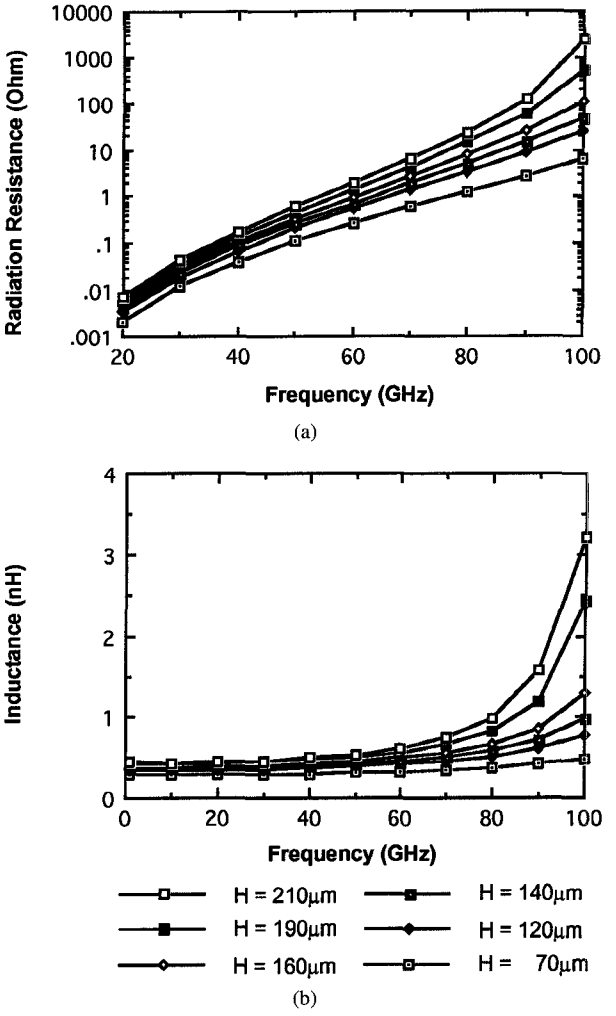

Fig. 5. Variations of (a) radiation resistance and (b) inductance of the grounded bonding wire to the bonding wire height (H= 70–210 m) from the bonding pad in Fig. 1.

of frequency using the Method of Moments by taking into account the ohmic loss using the Phenomenological Loss Equivalence Method. The radiation loss effect is observed to be significant and the wire inductance increases greatly due to the radiation effect above 30 GHz. The commonly used free-space static inductance (0.32 nH) of CAD software is overestimated 15% at low frequencies without considering the mutual inductance effect of the ground plane. The maximum quality factor is calculated to be about 150 at 40 GHz and the LC-resonance frequency is 97 GHz for a typical 70 μm $\times$ 70 μm bonding pad on a 100-μm-thick semi-insulating GaAs substrate. The bonding wire is highly reactive in most of the frequency range (DC to 100 GHz) while the maximum quality factor is limited by the ohmic resistance. Possible crosstalk due to the high radiation should be considered for interconnecting and packaging high-frequency integrated devices and circuits above 30 GHz. The wire height should be mainly minimized in order to reduce the radiation effect. This wideband characterization of the bonding wire is expected to be useful for accurate designs and characterizations of high frequency MMIC's and OEIC's. Finally, this approach can

be applied to wideband characterization of arbitrarily shaped interconnection wires for many high frequency integrated circuits.

REFERENCES

[1] E. F. Belohoubek, "Advanced microwave circuits," *IEEE Spectrum*, vol. 18, pp. 44–47, Feb. 1981.

[2] M. Nakamura, N. Suzuki, and T. Ozeki, "The superiority of opto-electronic integration for high-speed laser diode modulation," *IEEE J. Quantum Electron.*, vol. QE-22, pp. 822–826, June 1986.

[3] M. Schlechtweg, W. Reinert, P. J. Tasker, R. Bosch, J. Braunstein, A. Hülsmann, and K. Köhler, "Design and characterization of high performance 60 GHz pseudomorphic MODFET LNAs in CPW-technology based on accurate S-parameter and noise models," *IEEE Microwave and Millimeter-wave Monolithic Circuits Symp. Dig.*, Albuquerque, NM, 1992, pp. 29–32.

[4] *IEEE MTT-S Int. Microwave Symp., Proc. Joint Workshop on New Packaging Techniques for MMICs and Discrete Devices and Loss, Crosstalk, and Package Effects in Microwave and Millimeter-Wave Integrated Circuits*, Boston, MA, 1991.

[5] D. E. Carlton, K. R. Gleason, R. Hopkins, K. Jones, K. Noonan, and E. W. Strid, "Accurate measurement of high-speed package and interconnect parasitics," in *Proc. IEEE Custom Integrated Circuits Conf.*, Rochester, NY, 1988, pp. 23.3.1–23.3.7.

[6] R. Lane, "De-embedding device scattering parameters," *Microwave J.*, pp. 149–156, Aug. 1984.

[7] A. Sweet, *MIC & MMIC Amplifier and Oscillator Circuit Design.* Dedham, MA: Artech House, 1990, pp. 229–230.

[8] R. H. Caverly, "Characteristic impedance of integrated circuit bond wire," *IEEE Trans. Microwave Theory Tech.*, vol. MTT-34, pp. 982–984, Sept. 1986.

[9] E. F. Kuester and D. C. Chang, "Propagating modes along a thin wire located above a grounded dielectric slab," *IEEE Trans. Microwave Theory Tech.*, vol. MTT-25, pp. 1065–1069, Dec. 1977.

[10] H.-Y. Lee and T. Itoh, "Phenomenological loss equivalence method for planar quasi-TEM transmission line with a thin normal conductor or superconductor," *IEEE Trans. Microwave Theory Tech.*, vol. MTT-37, pp. 1904–1909, Dec. 1989.

[11] F. N. Sinnadurai, *The Handbook of Microelectronics of Packaging and Interconnections Technologies.* Electrochemical Publications, 1985.

[12] R. A. Pucel, "Design considerations for monolithic microwave circuits," *IEEE Trans. Microwave Theory Tech.*, vol. MTT-29, pp. 513–534, June 1981.

[13] H.-Y. Lee and T. Itoh, "Experimental and theoretical characterizations of very thin coplanar waveguide and coplanar slow-wave structures," *IEEE MTT-S Int. Microwave Symp. Dig.*, Dallas, TX, 1990, pp. 175–178.

[14] J. D. Welch and H. J. Pratt, "Losses in microstrip transmission line systems for integrated microwave circuits," *NEREM RECORD*, pp. 100–101, 1966.

[15] W. L. Stutzman and G. A. Thiel, *Antenna Theory and Design.* New York: John Wiley and Sons, Inc., 1981.

[16] J. C. Logan, "A Comparison of techniques for treating radiation and scattering by bent wire configurations with junctions," Syracuse University, Tech. Rep. TR-73-10, Aug. 1973.

[17] S. Ramo, J. R. Whinnery, and T. V. Duzer, *Fields and Waves in Communication Electronics.* New York: John Wiley and Sons, Inc., 1984, pp. 178–183.

[18] S. J. Haefner, "Alternating-current resistance of rectangular conductors," in *Proc. Institute of Radio Engineers*, vol. 25, no. 4, pp. 434–447, Apr. 1937.

[19] Touchstone, registered by EEsof, Inc., Westlake Village, CA.

[20] F. E. Gardiol, *Lossy Transmission Lines.* Dedham, MA: Artech House Inc., 1987.

[21] E. Pettenpaul, H. Kapuska, A. Weigerber, H. Mampe, J. Luginsland, and I. Wolff, "CAD models of lumped elements on GaAs up to 18 GHz," *IEEE Trans. Microwave Theory Tech.*, vol. MTT-36, pp. 294–304, Feb. 1988.

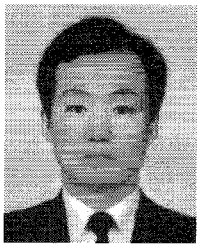

Hai-Young Lee (M '90) was born in Seoul, Korea, on March 7, 1957. He received the B.S. degree in electronics engineering from Ajou University, Suwon, Korea, in 1980, and the M.S. degree in electrical engineering from Korea Advanced Institute of Science and Technology, Seoul, Korea, in 1982. In 1989, he received the Ph.D. degree in electrical engineering from the University of Texas at Austin.

He was with the Ministry of National Defense, Korea, as a senior research engineer in the fields of electromagnetic compatibility and wave propagation from 1982 to 1986. From 1990 to 1992, he was in charge of the Advanced Research Section I working on MMIC and optoelectronic devices at the GoldStar Central Research Laboratory, Seoul, Korea. Since 1992, he has been with the Department of Electronics Engineering at Ajou University, Suwon, Korea, as an assistant professor. His current interest lies in the fields of design, packaging, and characterization of MMIC's and high-speed optoelectronic devices and also in superconductor applications for high-density interconnection lines.